RAPID COMMUNICATION

Mid-infrared free space wavelength beam splitter based on dual frequency reflective metalens

Japanese Journal of Applied Physics **61**, 080901 (2022) **RAPID COMMUNICATION**
https://doi.org/10.35848/1347-4065/ac7bc9

Mid-infrared free space wavelength beam splitter based on dual frequency reflective metalens

Boqi Wu[1], Yaodan Chi[1*], Hengxu Zhang[2], Chunlei Zhao[3], Yang Zhao[1], Sa Lv[1], and Jia Yang[1]

[1]*Department of Electrical and Computer science, Key Laboratory of the Ministry of Education for Comprehensive Energy Conservation in Cold Buildings, Jilin Jianzhu University, NO. 5088, Xincheng Street, Changchun, 130018, People's Republic of China*
[2]*Changchun China Optical Science and Technology Museum, NO. 1666 Yong Shun Road, Changchun, 130017, People's Republic of China*
[3]*Changchun Institute of Optics, Fine Mechanics and Physics, Chinese Academy of Sciences, No. 3888 Dong Nan Hu Road, Changchun, 130033, People's Republic of China*

[*]E-mail: xiancaitang@sina.com

Received May 24, 2022; revised June 17, 2022; accepted June 22, 2022; published online July 15, 2022

We present a reflective metalens with a hybrid antenna structure, which can realize the beam splitting function of two wavelengths in free space. A key feature of our design is the presence of phase-independent regulation at two different wavelengths in each nanoresonator, which can generate a specific phase or a continuous sweep in the range of 0° to more than 300°. To demonstrate the wavefront manipulation ability of the array, we simulated the characteristics of wavelength beam splitting, especially the free space wavelength beam splitter with a focal length of 300 μm and a relative focal position of 100 μm. © 2022 The Japan Society of Applied Physics

Supplementary material for this article is available online

The beam splitter is an optical component that can divide the incident light into different parts that propagate in different directions according to wavelengths, optical power, and polarization direction.[1–6] With this function, it can be used in many fields, such as spectral imaging,[7] sensing technology,[8] solar cell design,[9] and optical communication.[10] The recent rise of miniaturized optical equipment also puts forward the requirements of chip-scale integration for this kind of optical element.

To meet this demand, the use of metasurfaces has been explored.[11–13] The metasurface is an ultra-thin artificial material that can manipulate the phase, amplitude, and polarization of electromagnetic waves by changing the structural size[14] or external modulation conditions, such as voltage,[15] temperature,[16] and magnetic field.[17] Pioneering studies on beam splitters exploited various metasurfaces and sub-wavelength gradient antenna structures. K. Wen et al.[18] have proposed a plasmonic T-shaped metal–insulator–metal waveguide followed by two or four output waveguides with ultranarrow silica slits to serve as an optical power and wavelength splitter in a compact footprint. X. Deng et al.[19] have realized the wavelength splitting by the metal grating with different grating periods and fill factors on the left and right half. González-Andrade D. et al.[20] have presented an ultra-broadband polarization-insensitive optical power splitter with relaxed fabrication tolerances by exploiting modal engineering in slotted waveguides. However, most beam splitters mainly focus on beam splitting of optical power and polarization.[21,22] The research on wavelength beam splitters is rarely involved, and most of them are mainly realized in waveguide mode rather than in free space. Moreover, most beam splitters focus on infrared, visible, and telecommunication frequencies, but few related studies in the mid-infrared band are of great significance in target detection, thermal imaging, and various medical fields.

By producing a hyperbolical phase profile, metasurfaces can work as lenses (also referred to as metalenses) that can control the wavefront and polarization of light. Here, we present a dual-frequency reflective metalens composed of a dual structure hybrid antenna array designed to demonstrate the function of free-space wavelength splitting in the mid-infrared regime. The phase coefficients corresponding to different positions of the metalens can be tuned by changing the relative size of the two plasmonic nanoresonators. Utilizing the key dimensional features of two structures as two separate control knobs, we achieve completely independent control of the phase over 300° in two wavelengths independently. Detailed numerical investigations reveal that the metalens with specific phase distribution simultaneously allows us to focus and split the incident light into two mid-infrared bands. By changing the phase distribution of the metalens, we obtain the focusing effect with the focal length of 200–400 μm and the wavelength splitting effect with the relative distance of 60–200 μm. This ultracompact wavelength splitter is significant for detecting techniques and medical applications in the mid-infrared band.

To achieve the focusing effect, the phase of the metalens needs to be set to a specific phase profile such that the beams reflected from individual pixels are in phase at the desired focal point. For this purpose, the phase shift provided by the metalens is determined by the hyperboloid profile:[23]

$$\varphi(x, y, f) = \frac{2\pi}{\lambda}\left(\sqrt{(x - x_0)^2 + (y - y_0)^2 + f^2} - f\right), \quad (1)$$

where λ is the wavelength, f is the focal length, x_0, y_0 are center position coordinates, and x, y is the distance of the pixel from the center of the lens. In the process of metalens design, because the unit resonant structure has a certain area, the continuous phase distribution in Eq. (1) must be discretized with the periodic parameters of the metalens. In this paper, we assume the periods of the metalens structure along the x and y directions are the same, and its discrete phase distribution can be expressed as:

$$\varphi(m, n, f) = \frac{2\pi}{\lambda}\left(\sqrt{(mp - x_0)^2 + (np - y_0)^2 + f^2} - f\right), \quad (2)$$

where m and n are integers that represent the structural unit code of the metalens in the x and y directions, respectively, and p represents the unit period of the metalens.

According to Eqs. (1) and (2), the metalens must meet the phase profiles for different focus positions at both

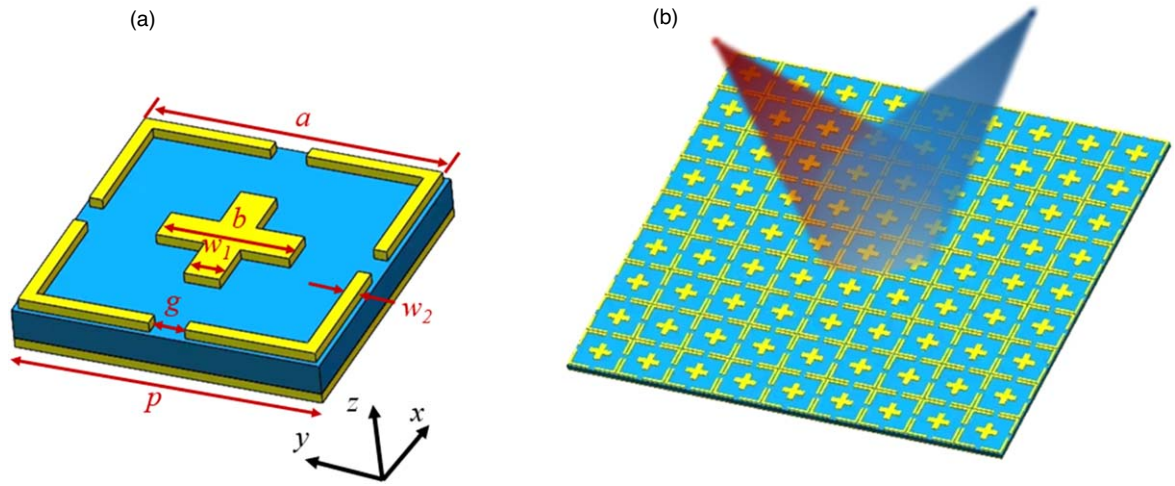

Fig. 1. (Color online) (a) Schematic of the designed unit cell; (b) schematic of the structure array of the designed 3D metalens.

wavelengths to realize dual-wavelength beam splitting. Therefore, we combine the traditional cross structure and square resonant ring structure into a new dual-frequency reflective metalens unit structure, as shown in Fig. 1(a). The metalens is composed of an Au back-reflector, an Al_2O_3 dielectric layer, and an Au hybrid structure antenna. The periodicity of the metalens is $p = 3$ μm, and the thickness of the back-reflector, antenna, and Al_2O_3 layers are $t_{back} = 0.01$ μm, $t_{antenna} = 0.01$ μm, and $t_{dielectric} = 0.35$ μm, respectively. The initial detailed structural parameters of the antenna are $a = 2.1$ μm, $b = 1.2$ μm, $g = 0.35$ μm, $w_1 = 0.35$ μm, and $w_2 = 0.13$ μm. The material properties of Au can be expressed in the mid-infrared band by the following formula:[24)]

$$\varepsilon_m(\omega) = 1 - \frac{\omega_p^2}{\omega(\omega + i\omega_c)}, \tag{3}$$

where the plasma frequency $\omega_p = 1.37 \times 10^6$ rad s^{-1} and the collision frequency $\omega_c = 4.07 \times 10^{13}$ rad s^{-1}. Additionally, we set the x and y direction boundary as the unit cell boundary and set the z direction boundary as the PML (perfectly matched layer) boundary in the Lumerical FDTD solutions software. The direction and the polarization of the incident light are set to $-z$ and E_x, which means that the electric field direction is parallel to the x-axis.

Ideally, to obtain the target phase profile, we need the antenna unit to realize 360° phase scanning by changing the structural parameters. Therefore, we first simulated the metalens unit under different structural parameters and obtained its reflectivity curves and phase curves, as shown in Fig. 2. The black curves with blocks in Fig. 2 are the reflectivity curves and phase curves under the initial structural parameters. The antenna array under this structural parameter has two resonance points at both 3.80 and 4.75 μm, which is also the trough of reflectivity and the abrupt change of phase. When we only change the length of the cross (b) to 1.2 μm, the reflectivity and phase at 4.75 μm will not change. However, at the same time, the resonance points at 3.80 μm will shift red, and its new resonance point will shift to 4.1 μm, which leads to the change of the corresponding phase value. Similarly, when the square ring (a) length is changed to 2.2 μm, the resonance point on the left remains unchanged, while the resonance point on the right is offset to 5.18 μm.

Then, to more clearly explain the reason for the shift of the resonant point, we simulate the electric field under the above dimensions, as shown in the illustration in Fig. 2(a). For the curve with a black block, the electric field distribution diagram shows that when the incident wavelength is 3.8 μm, the electric field will concentrate on the left and right ends of the cross structure, which indicates that the electric dipole resonance occurs at this position. This phenomenon leads to the abrupt change of the designed structure's reflection curve and phase curve at this wavelength. When the incident wavelength is 4.75 μm, the electric field aggregation effect and electric dipole resonance will also occur, except that the position at this time is transferred to the opening of the square ring resonator. The electric field aggregation effect at these two different positions endows the structure with the ability of phase mutation at both wavelengths. When we change the structural parameters of a and b, the electric field aggregation distribution will appear at the new resonance wavelength, as shown in Fig. S1 (available online at stacks.iop.org/JJAP/61/080901/mmedia), which is the reason for the position of phase mutation and the change of phase at a fixed wavelength.

Figure 2(b) is enough to prove that the function of dual-wavelength phase modulation can be obtained by changing the parameters of the two structures, respectively. Therefore, we simulate and extract the phases corresponding to different structural parameters under $\lambda = 4.0$ μm and $\lambda = 5.5$ μm, respectively, as shown in Fig. 3. When only the structural parameters of the cross (a) change, the phase at $\lambda = 5.5$ μm will shift, while the phase at $\lambda = 4.0$ μm will hardly change. On the contrary, when only the structural parameters of the square ring (b) change, only the phase at $\lambda = 4.0$ μm will respond to it. At the same time, the corresponding reflectivity will also change regularly, as shown in Figs. 3(c), 3(d). The in-depth simulation results show that the maximum phase modulation range at $\lambda = 4.0$ μm can reach 310°, and the phase modulation range at $\lambda = 5.5$ μm can also reach the level of 300°. Using this dual-wavelength phase modulation function and significant phase modulation range, we can determine the corresponding structural parameters at any

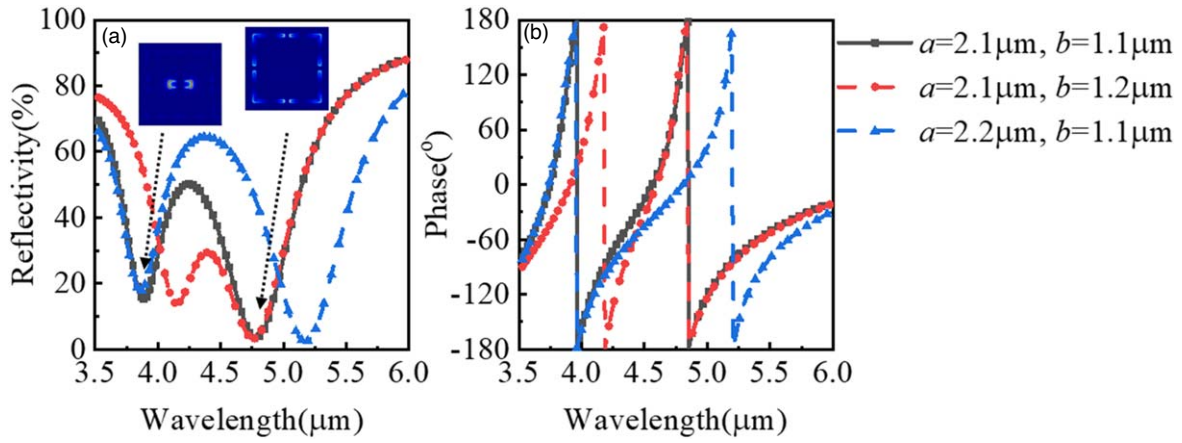

Fig. 2. (Color online) (a) Reflectivity curves (the illustration shows the electric field distribution at two resonant wavelengths) and (b) phase curve under different structural parameters.

position of the metalens to meet the requirements of different phases at two wavelengths simultaneously.

We designed a set of metalens with focal lengths from $f = 400\,\mu$m down to $f = 200\,\mu$m in $100\,\mu$m steps, which corresponded to the relative position difference of beam focusing position (d_x) from $d_x = 100$ to $d_x = 200\,\mu$m. Taking $f = 300\,\mu$m and $d_x = 100\,\mu$m as examples, we first calculate the phase curves of the wavelengths are 4.0 μm and 5.5 μm when x_0 is $-50\,\mu$m and $50\,\mu$m according to Eqs. 1 and 2, as shown in Fig. S2. Secondly, according to the two curves and the results of Fig. 3, we find the structural parameters that can meet the phases of two incident waves at the same time in different x coordinates. Finally, the element structures corresponding to the structural parameters of the phase curve are arranged along the x-axis. In addition, similar steps are also done for other structures on the y-axis. Only the value of y_0 needs to be changed. It should be noted that the designed structure is rotationally symmetrical, so the incident light in E_x and E_y polarization directions has the same wavelength division effect. In this simulation process, we mainly take E_x polarization as an example. As shown in Fig. 4, when the light of two wavelengths is incident on the surface of the designed metalens, similar to the focal length ($f = 300\,\mu$m) and beam focusing position distance ($d_x = 100\,\mu$m) calculated in advance, there is a reflection focus at positions (150 μm, 280 μm) and (230 μm, 280 μm) on the x–z plane, respectively. Although the focal length and focus position are slightly offset because the modulation range of the phase cannot reach the complete 360°, and the gradient can only take the phase curve. The phenomenon shown in Fig. 4 is enough to prove that the designed metalens can realize the function of a wave splitter. Moreover, this offset can be compensated and adjusted according to the needs of subsequent practical applications. In addition, as shown in Fig. S3, by changing the parameters and arrangement of the unit structure, the beam splitting function of different wavelengths can be realized at different focal lengths, and the beam splitting position can be adjusted accordingly. It should be noted that the size of the metalens needs to be corrected according to the focal length and beam splitting position.

To further verify the generality of this design method of wavelength division devices, we designed a three-dimensional (3D) metalens with beam splitting at any focusing position. Here, based on Eqs. (1)), we set the focal length as 300 μm and set the focusing points as (130 μm, 180 μm) and (230 μm, 180 μm) on the x–y plane, which indicates the focusing position on the focusing plane for the incident light of $\lambda = 4.0\,\mu$m and $\lambda = 5.5\,\mu$m, respectively. The reflected light intensity distributions in the focal plane are demonstrated in Figs. 5(a), 5(b). The results show that the designed 3D metalens can be used as a wavelength beam splitter to focus the incident light of two different wavelengths at different positions in free space. Figure 5(c) illustrates the normalized reflected intensity distribution in the focal plane in case of the light incidence of $\lambda = 4.0\,\mu$m and $\lambda = 5.5\,\mu$m. There is only a slight difference of about 5% in the light intensity of the focused beam profile corresponding to the two wavelengths. The FHWM of the two focused spots is 4.96 μm and 4.85 μm, respectively, almost reaching their diffraction limits (λ/2NA). In addition, the focusing efficiency and extinction ratio of 3D metalens beam splitter at two wavelengths can reach 30.2%, −22 dB, and 33.1%, −24 dB, respectively. The main reason for the low focusing efficiency is that the metalens unit structure with some structural parameters has the problem of low reflectivity, which is also the disadvantage of the resonance phenomenon of reflective metalens. In the future, we plan to design a metalens structure unit that can simultaneously achieve fixed phase value and high reflectivity at the target wavelength through machine learning and reverse design.

In addition, taking the designed metalens as the starting point, we can realize the design of a parallel light wavelength division device, which only needs to change the phase distribution. This function is mainly realized based on the wavefront controller of beam deflection, and its phase distribution can be expressed as:[25)]

$$\varphi(x) = k_0 x \sin\theta = \frac{2\pi}{\lambda_0} x \sin\theta, \tag{4}$$

where x is the relative position, k_0 is the wavenumber, λ_0 is the wavelength of the incident light, θ is the target incidence angle, $\varphi(x)$ is the phase of the desired position. Fig. S4 shows the far-field distribution of the metalens with incident wavelengths of 4.0 and 5.5 μm and phase gradients of 60° and −60°, respectively. The reflection deflection angles at these two wavelengths are 14.2° and −16.0°, respectively,

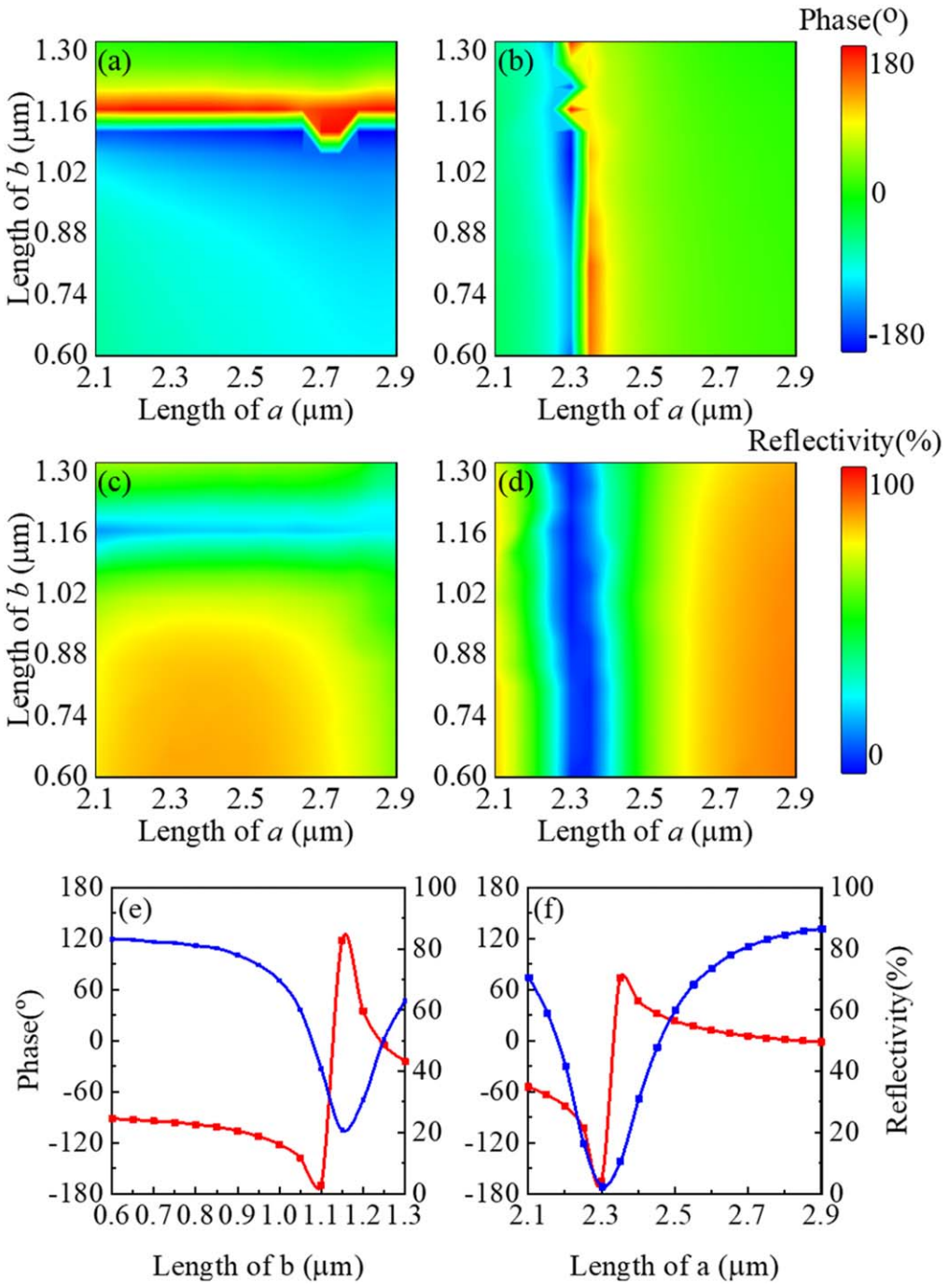

Fig. 3. (Color online) Reflection phase and reflectivity contours under different structural parameters when the incident wavelengths are (a), (c) $\lambda = 4.0$ μm and (b), (d) $\lambda = 5.5$ μm, respectively. Reflectivity curve and phase curve under the structural parameters of (e) $a = 2.5$ μm, $b = 0.6$–1.3 μm, $\lambda = 4.0$ μm and (f) $a = 2.1$–2.9 μm, $b = 1.0$ μm, $\lambda = 5.5$ μm.

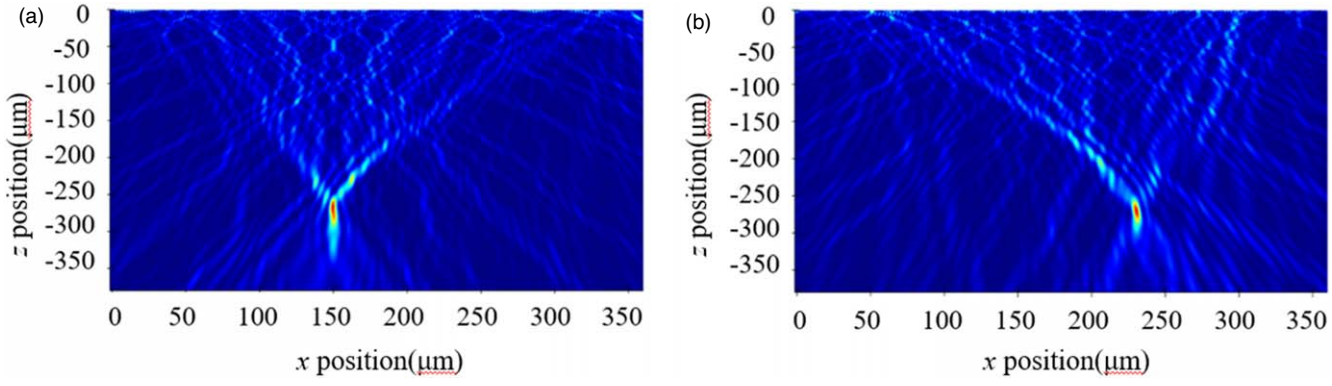

Fig. 4. (Color online) Intensity distribution of reflected light with incident wavelengths of (a) $\lambda = 4.0$ μm and (b) $\lambda = 5.5$ μm under the same metalens array.

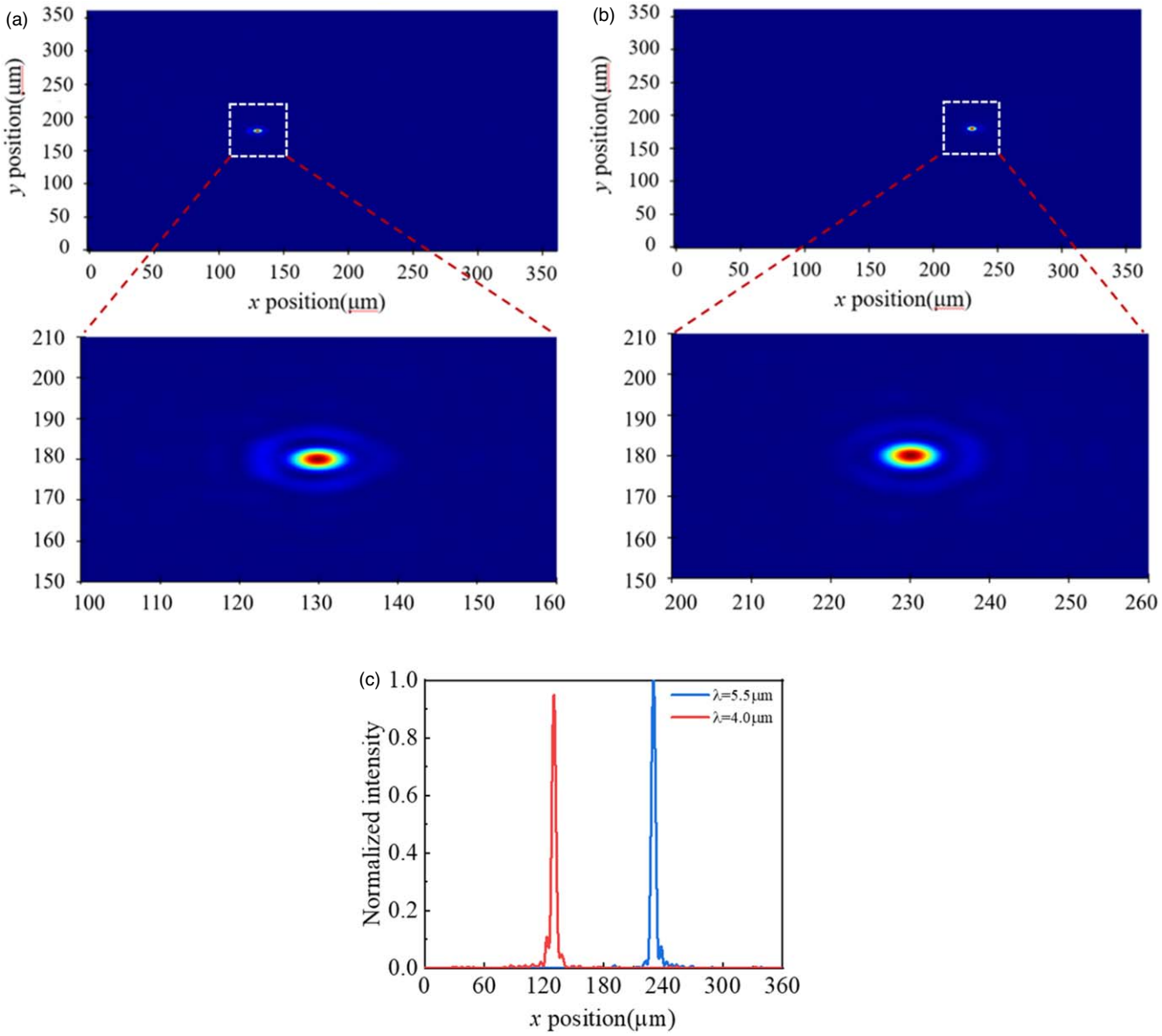

Fig. 5. (Color online) Reflected light intensity with incident wavelengths of (a) $\lambda = 4.0$ μm and (b) $\lambda = 5.5$ μm and (c) light intensity profile distribution on focal plane under the same metalens array.

and the asymmetry of the two angles is mainly due to the slight difference in the deflection angles corresponding to different wavelengths under the same phase gradient, which can be obtained according to Eq. (3). In addition, it can be observed from Fig. S4(b) that there are some unnecessary side lobes in the far-field distribution, which is mainly caused by the inability of the phase regulation range of the metalens unit structure to reach 360°. However, through detailed simulation, it is found that the maximum energy of these side lobes is only 18% of the energy of the main lobe, which will only have a limited subtle impact on practical applications.

In conclusion, we have shown a free space wavelength splitter based on a dual-wavelength reflective metalens and demonstrated two-wavelength beam manipulation in the mid-infrared regime. With the hybrid dual structure antenna, we accomplished independent modulation of the phase over 300° at dual-wavelength. The wavelength beam splitter based on the designed 3D metalens can achieve a focal length of 300 μm, a relative focus position of 100 μm, and FWHM of about 4.90 μm. The focal length and relative focus position can be further adjusted by changing the phase distribution curve of the metalens array. The proposed splitter is compact and fabricated, which can be used in integrated optical systems on a subwavelength scale.

Acknowledgments This research was sponsored by the Science and Technology Department of Jilin Province(20210203164SF).

1) D. Dai, Z. Wang, J. Peters, and J. E. Bowers, "Compact polarization beam splitter using an asymmetrical mach–zehnder interferometer based on silicon-on-insulator waveguides," IEEE Photonics Technol. Lett. **24**, 673 (2012).
2) S. Hu, S. Du, J. Li, and C. Gu, "Multidimensional image and beam splitter based on hyperbolic metamaterials," Nano Lett. **21**, 1792 (2021).
3) J. Huang, J. Yang, D. Chen, X. He, Y. Han, J. Zhang, and Z. Zhang, "Ultra-compact broadband polarization beam splitter with strong expansibility," Photonics Res. **6**, 574 (2018).
4) X. Liu, D. Liu, and D. Dai, "Silicon polarization beam splitter at the 2 μm wavelength band by using a bent directional coupler assisted with a nano-slot waveguide," Opt. Express **29**, 2720 (2021).

5) A. Ozer, N. Yilmaz, H. Kocer, and H. Kurt, "Polarization-insensitive beam splitters using all-dielectric phase gradient metasurfaces at visible wavelengths," Opt. Lett. **43**, 4350 (2018).
6) F. Ding, R. Deshpande, and S. I. Bozhevolnyi, "Bifunctional gap-plasmon metasurfaces for visible light: polarization-controlled unidirectional surface plasmon excitation and beam steering at normal incidence," Light: Sci. Appl. **7**, 17178 (2018).
7) R. H. Berg, "Evaluation of spectral imaging for plant cell analysis," J. Microsc. **214**, 174 (2004).
8) S. Koyama, K. Onozawa, K. Tanaka, S. Saito, S. M. Kourkouss, and Y. Kato, "Multiocular image sensor with on-chip beam-splitter and inner meta-micro-lens for single-main-lens stereo camera," Opt. Express **24**, 18035 (2016).
9) K. P. Sibin, N. Selvakumar, A. Kumar, A. Dey, N. Sridhara, H. D. Shashikala, A. K. Sharma, and H. C. Barshilia, "Design and development of ITO/Ag/ITO spectral beam splitter coating for photovoltaic-thermoelectric hybrid systems," Sol. Energy **141**, 118 (2017).
10) Z. Gong, R. Yin, W. Ji, J. Wang, C. Wu, X. Li, and S. Zhang, "Optimal design of DC-based polarization beam splitter in lithium niobate on insulator," Opt. Commun. **396**, 23 (2017).
11) M. Khorasaninejad, W. Zhu, and K. B. Crozier, "Efficient polarization beam splitter pixels based on a dielectric metasurface," Optica **2**, 376 (2015).
12) J. H. Lee, J. Woong Yoon, M. Jin Jung, J. Kyun Hong, S. Ho Song, and R. Magnusson, "A semiconductor metasurface with multiple functionalities: A polarizing beam splitter with simultaneous focusing ability," Appl. Phys. Lett. **104**, 233505 (2014).
13) X. Zhang, R. Deng, F. Yang, C. Jiang, S. Xu, and M. Li, "Metasurface-based ultrathin beam splitter with variable split angle and power distribution," ACS Photonics **5**, 2997 (2018).
14) Y. F. Yu, A. Y. Zhu, R. Paniagua-Domínguez, Y. H. Fu, B. Luk'yanchuk, and A. I. Kuznetsov, "High-transmission dielectric metasurface with 2π phase control at visible wavelengths," Laser Photonics Rev. **9**, 412 (2015).
15) Y.-W. Huang, H. W. H. Lee, R. Sokhoyan, R. A. Pala, K. Thyagarajan, S. Han, D. P. Tsai, and H. A. Atwater, "Gate-tunable conducting oxide metasurfaces," Nano Lett. **16**, 5319 (2016).
16) W. Li and Y. Cheng, "Dual-band tunable terahertz perfect metamaterial absorber based on strontium titanate (STO) resonator structure," Opt. Commun. **462**, 125265 (2020).
17) X. Chen, P. Liu, Z. Hou, and Y. Pei, "Magnetic-control multifunctional acoustic metasurface for reflected wave manipulation at deep subwavelength scale," Sci. Rep. **7**, 9050 (2017).
18) K. Wen, Y. Hu, L. Chen, J. Zhou, L. Lei, and Z. Guo, "Design of an optical power and wavelength splitter based on subwavelength waveguides," J. Lightwave Technol. **32**, 3020 (2014).
19) Y. Yu, C. Sun, J. Li, and X. Deng, "A plasmonic metal grating wavelength splitter," J. Phys. D: Appl. Phys. **48**, 015102 (2014).
20) D. González-Andrade et al., "Polarization- and wavelength-agnostic nano-photonic beam splitter," Sci. Rep. **9**, 3604 (2019).
21) S. Boroviks, R. A. Deshpande, N. A. Mortensen, and S. I. Bozhevolnyi, "Multifunctional metamirror: polarization splitting and focusing," ACS Photonics **5**, 1648 (2018).
22) F. Ding, Y. Chen, and S. I. Bozhevolnyi, "Gap-surface plasmon metasurfaces for linear-polarization conversion, focusing, and beam splitting," Photonics Res. **8**, 707 (2020).
23) S. Wang et al., "A broadband achromatic metalens in the visible," Nat. Nanotechnol. **13**, 227 (2018).
24) T.-T. Kim, H.-D. Kim, R. Zhao, S. S. Oh, T. Ha, D. S. Chung, Y. H. Lee, B. Min, and S. Zhang, "Electrically tunable slow light using graphene metamaterials," ACS Photonics **5**, 1800 (2018).
25) J. Park et al., "All-solid-state spatial light modulator with independent phase and amplitude control for three-dimensional LiDAR applications," Nat. Nanotechnol. **16**, 69 (2021).